Layer-by-layer versus surfactant dissolution modes in heteroepitaxy

Jean-Marc Roussel, Andrés Saúl, and Guy Tréglia
CRMC2-CNRS, Campus de Luminy, Case 913, 13288 Marseille Cedex 9, France

Bernard Legrand
SRMP/DECM, CEA Saclay, 91191 Gif-sur-Yvette Cedex, France
(Received 18 May 1999)

Dissolution of a thick A film into a B substrate during metal heteroepitaxy (A/B) obeys general trends which are described here in the case where the corresponding AB alloy presents a tendency to bulk phase separation and to B surface segregation (e.g., $A=$Ni, $B=$Ag). Using the kinetic tight-binding Ising model, either in the mean-field or in the Monte Carlo framework, we find *layer-by-layer* dissolution modes which, depending on the annealing temperature T, are preceded ($T>T_k$) or not ($T<T_k$) by the rising of capping B monolayers burying an almost intact A film (*surfactantlike* effect). T_k is found to decrease as the tendency to surface segregation of the substrate element increases, which can be understood in terms of local equilibrium at both the surface and the interface of the deposit. The model gives access to the main kinetic laws which are obeyed in the two dissolution modes, i.e., the total quantity of deposit matter decreases linearly with the square root of time. [S0163-1829(99)00243-X]

I. INTRODUCTION

During metal-on-metal heteroepitaxy, some interdiffusion can occur at intermediate temperatures between the deposited and substrate elements, which remains limited in the surface selvedge. This can lead to the formation of metastable surface alloys or to some unusual dissolution modes, complementary to the usual growth ones.[1] These clearly non-Fickian modes are tightly linked to the main features of the surfaces of the alloyed systems made of the two elements (deposit and substrate), namely, to the tendency of either the deposit or the substrate species to segregate at the surface and of the bulk system to either form ordered phases or to phase separate. Thus, when the ''deposit-substrate'' couple presents a tendency to bulk ordering, the dissolution can be blocked on ordered compounds, similar or not to the bulk ones but confined near the surface.

When the couple presents a tendency to bulk phase separation, different situations can occur, depending on the tendency of either the deposited or the substrate element to segregate at the surface and on the number of deposited monolayers. When the deposited element has a strong tendency to segregate (for example Ag/Cu), and in the case of a thin deposit (1 ML), it has been shown experimentally[2] and theoretically[3] that the concentration of the deposited element at the surface decreases linearly with the square root of time. The same system has been studied theoretically for a thicker deposit (10 ML).[4] The study has shown that the dissolution occurs layer-by-layer, i.e., each deposit layer dissolves successively starting from the layer at the deposit-substrate interface.

On the other hand, when the substrate element has a strong tendency to segregate (for example Ni/Ag), the kinetics may reveal a ''surfactantlike'' behavior which consists of the climb of the substrate element through the deposit to the surface.[5] Thus, the deposit layers can be buried below some floating monolayers, and this surfactant effect can also persist during the growth as has been shown experimentally. Numerous experimental and theoretical studies have been devoted to systems which are candidate to present such a surfactantlike behavior. For example, a thin initial deposit (1–2 ML) of Cu on Pb (Ref. 6) or Ni on Ag (Refs. 5, 7, and 8) has given rise to the formation of embedded clusters immersed under one or two capping substrate monolayers. In this case, the thickness of the initial deposit plays a crucial role on the kinetics and in particular on the microstructure obtained for the encapsulated deposit. For instance, recent experimental results have shown that the annealing of a thick deposit may lead to the climbing of substrate atoms to the surface which seems to leave the morphology of the buried film intact [Rh/Ag,[9] Fe/Cu,[10] Co/Cu (Refs. 11 and 12)].

The aim of this work is to study this latter situation by considering the dissolution modes of a thick deposit (10 ML) for systems which present a phase-separation tendency, a size mismatch, and a surface energy difference that do not retain the deposit at the surface, so that they should present a surfactantlike effect. We will focus on systems with the fcc structure and a (100) surface orientation.

All these behaviors can be modeled in the framework of the kinetic tight-binding Ising model (KTBIM),[13,14] which takes into account the main driving forces of the phenomena. These driving forces include a term $V<0$ which gives the strength of the phase separation and a term $\Delta\tau$ which gives the tendency of either the substrate element ($\Delta\tau>0$) or the deposit one ($\Delta\tau<0$) to segregate to the surface. This latter term corresponds to a global contribution related to both the difference in surface energy and in lattice parameter between the two elements.

For the sake of clarity of the paper, and in order to emphasize its main contribution, before presenting details of our calculations we will give in the following section (Sec. II) an outline of the essential trends so-derived in a qualitative form.

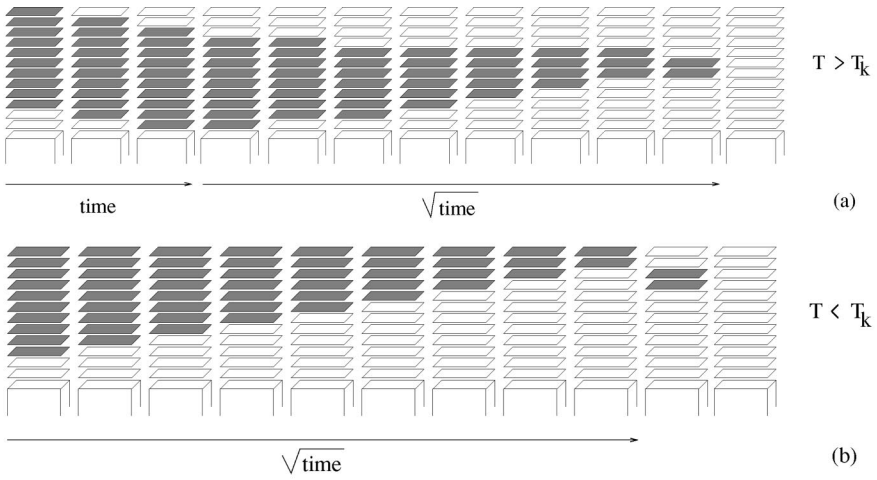

FIG. 1. Schematic time evolution of the dissolution of a thick 10 ML deposit as a function of the temperature; the A deposit layers are in gray and the B substrate ones in white. The upper sketch (a) represents the surfactant-layer-by-layer mode observed for $T>T_k$. At the beginning of the dissolution the images are spaced linearly in t and then linearly in $\sqrt{t}$. The lower sketch (b) corresponds to the layer-by-layer mode occurring for $T<T_k$. Again each image represents a snapshot taken at constant steps in $\sqrt{t}$.

II. QUALITATIVE SURVEY OF THE MAIN TRENDS

Following the terminology used by Pandit *et al.* in Ref. 15 for multilayer adsorption phenomena, one can similarly distinguish three broad classes of systems: $\Delta\tau \gg \Delta\tau_k$ corresponding to *strong-segregation* systems; $0<\Delta\tau<\Delta\tau_k$ which we shall call *intermediate-segregation* systems; and $\Delta\tau\sim 0$ which we shall call *weak-segregation* systems. $\Delta\tau_k$ is a critical value of the surface segregation term equal to $-Z'V$ in the terminology of Ref. 15. We will also show in the following that $\Delta\tau_k=-(Z'+Z)V_0+ZV$, if a different value V_0 of the parameter controlling the phase separation strength is used near the surface. Here Z' is the number of first-neighbors broken bonds at the surface, Z the number of first neighbors in the same plane [$Z=Z'=4$ for the fcc(100) orientation], and in this paper we will consider only the case $V,V_0<0$. Let us note that the terms strong, weak, or intermediate qualify the surface segregation of the substrate atoms (majority elements) with respect to the deposit ones (minority ones). The reason for using this convention instead of the usual one, qualifying the segregation of the minority element, will be clear in Sec. IV B 2.

Figures 1 show the schematic dissolution modes of a 10 ML deposit of an A element on a B substrate as a function of the annealing temperature and for a fixed value of $\Delta\tau$ in the intermediate regime. The simulations put in evidence the existence of a critical temperature T_k that delimits two distinct dissolution domains, namely, a *surfactant-layer-by-layer* mode for $T>T_k$ and a *layer-by-layer* one for $T<T_k$.

In the high-temperature domain $T>T_k$ [see Fig. 1(a)], starting from a $\{A/A/\ldots/A/B/\ldots\}$ profile, we rapidly obtain a surface enrichment in B giving rise to a $\{B/B/A/A/\ldots/A/B/\ldots\}$ profile (surfactantlike effect). During this short stage the loss of A matter into the bulk is negligible. Then, the dissolution occurs layer-by-layer alternately from the top or the bottom of the deposit until a $\{B/B/B/B/B/A/A/B/\ldots\}$ profile is reached. Finally, the last two A layers disappear in the bulk much more rapidly than the previous ones. Using both mean-field and Monte Carlo simulations, we recover the same features for the evolution of the dissolution mode. In particular, both methods predict for a thick deposit that the surfactantlike effect proceeds by conserving abrupt A/B interfaces.

In the low-temperature domain $T<T_k$ [see Fig. 1(b)], the dissolution mode is drastically changed. Starting again from a $\{A/A/\ldots/A/B/\ldots\}$ profile, we do not observe any B enrichment at the surface. The dissolution obeys a layer-by-layer mode now *only* located at the deposit/substrate interface. Finally when a $\{A/A/B/B/\ldots\}$ profile is achieved, the two remaining A layers are immersed under two capping B layers and then are dissolved rapidly.

Even though these dissolution modes are clearly non-Fickian, we will show that the different stages illustrated in Fig. 1 are in fact driven by some very small concentrations of the order of the bulk solubility limit c_α and that they follow the Fick's equations. This observation will allow us to derive the kinetic laws obeyed during the different stages, namely, the surfactant behavior occurring at the high-temperature regime, and the layer-by-layer modes taking place either after this stage or in the low-temperature regime. A full understanding of the kinetic behaviors (dissolution modes, kinetic laws, and the critical temperature T_k) as a function of the nature of the system requires to invoke a *local equilibrium* concept,[16] i.e., the existence of a ''derm'' (whose thickness has to be defined) which remains in equilibrium with the surface planes during the kinetics of surface segregation or dissolution. Thus the kinetics may be completely or partly driven by this surface region in local equilibrium (the derm) in which metastable branches can have a dominant role. This local equilibrium concept can be also used to show that the enrichment of the surface in B elements when the surfactant effect takes place is linear with the time t,[17] and that during the layer-by-layer dissolution the total loss of A matter obeys a $\sqrt{t}$ law:

$$M(t)=M(0)-2c_\alpha\sqrt{\frac{t}{\pi t_0}}, \tag{1}$$

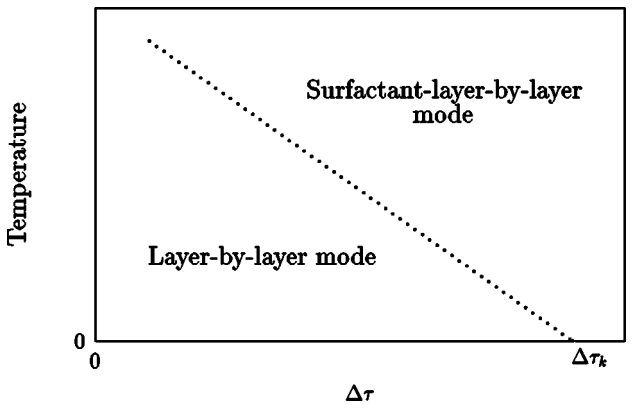

FIG. 2. Schematic map describing the dependence of the dissolution modes as a function of the annealing temperature and the driving forces for the surface segregation of the substrate atoms ($\Delta\tau$). The dotted T_k line delimits the two domains and $\Delta\tau_k$ refers to the boundary between intermediate and strong segregation systems (see text).

where $M(0)$ is the initial number of monolayers in the thick deposit, $t_0=d^2/D$, D the diffusion coefficient, and d the interplanar distance.[17]

Finally, we will present qualitatively the influence of the surface driving forces $\Delta\tau$ on the value of the critical temperature delimiting the dissolution domains. As defined above, $\Delta\tau$ gives the tendency of the substrate element to segregate ($\Delta\tau>0$) or not ($\Delta\tau<0$). Figure 2 gives the main trends derived from the simulations. We find that decreasing $\Delta\tau$ leads to an increase of the critical temperature delimiting the two dissolution domains. In addition, we will show that the T_k line is lower in Monte Carlo than in mean field, but in both cases it reaches the same critical value $\Delta\tau_k$ (at $T_k=0$) giving the boundary between the intermediate and the strong regime. Thus, in the strong regime, only the *surfactant-layer-by-layer* mode is observed. The kinetic transition at T_k will be described in detail and explained in terms of local equilibrium as a coupling between the surface isotherms shown in Sec. IV A and the shape of the deposit/substrate interface. Thus the above-mentioned ''derm'' will have to include the A/B interface. The same feature is found from the Monte Carlo simulations and detail of the corresponding $(\Delta\tau,T)$ structural map will be developed in Sec. IV C.

III. MODEL

A. Hamiltonian

Since the basis of the model has been described in several articles,[13,14] only a brief survey will be given here. The energetics used in the kinetic model is based on an effective Ising Hamiltonian derived from electronic structure calculations (TBIM) for surface segregation problems. The grand-canonical Hamiltonian of a semi-infinite alloy within the TBIM can be written as

$$\tilde{H}^{\mathrm{TBIM}}=\sum_n p_n\left\{\Delta h_n^{\mathrm{eff}}+\Delta H_n^{\mathrm{size}}-\sum_{m\neq n} V_{nm}-\mu\right\}+\sum_{n,m\neq n} p_n p_m V_{nm}, \tag{2}$$

where p_n is the spinlike occupation variable equal to 1 or 0 if the site n is occupied by an atom A or B, respectively, and μ is the difference in chemical potentials. The energetic parameters are as follows.

(i) V_{nm} which is the effective pair interaction between atoms at sites n and m. For fcc structures it is negligible beyond first neighbors: $V_{nm}=V$ if n,m are first neighbors and $V_{nm}=0$ if not.[18] V is directly related to the bulk phase diagram of the system considered. Its sign gives the tendency to ordering ($V>0$) or phase separation ($V<0$). It is worth noticing that when at least one site belongs to the surface, the interaction V is enhanced. $V_0=1.5$ V for the (100) fcc surface.[19]

(ii) $\Delta h_n^{\mathrm{eff}}$ which is a surface contribution: it is found very close to the difference in surface energies between the pure constituents if the site n belongs to the surface (that we will denote $\Delta h_0^{\mathrm{eff}}$ in the following) and to vanish otherwise.

(iii) $\Delta H_n^{\mathrm{size}}$ which accounts for the size-mismatch between the two constituents: it also vanishes except if n belongs to the surface (we will call it $\Delta H_0^{\mathrm{size}}$ in the following), in which case it is calculated by means of a tight-binding quenched molecular dynamics using a ''second moment potential.''[20,21] In this scheme $\Delta H_0^{\mathrm{size}}$ is calculated as the size-dependent part of the segregation energy involved when a single impurity is moved from the totally relaxed bulk to the totally relaxed surface. Such a calculation shows that, contrary to usual elasticity theory, the size effect should induce the segregation of the impurity at the surface *only* if it is the largest. Note, however, that the use of such an impurity calculation can be criticized in the case of strong surface segregation or of dissolution. Indeed in this latter case, when the deposit thickness increases, substrate atoms behave more and more as minority atoms in the deposit, while the $\Delta H_0^{\mathrm{size}}$ term still refers to deposit elements (which are minority ones with respect to the substrate). In the present work, we will then allow this $\Delta H_0^{\mathrm{size}}$ term to vary. In practice we will consider the sum $\Delta\tau=\Delta h_0^{\mathrm{eff}}+\Delta H_0^{\mathrm{size}}$ as a global surface contribution, the sign of which gives the tendency of either the substrate element ($\Delta\tau>0$) or the deposit one ($\Delta\tau<0$) to segregate to the surface.

Let us recall that the $\tilde{H}^{\mathrm{TBIM}}$ is equivalent to the lattice gas Hamiltonian or the spin-$\frac{1}{2}$ Ising one. For nearest-neighbor interactions only, $\tilde{H}^{\mathrm{TBIM}}$ gives the whole phase diagram reflection symmetry in the line $\Delta\tau=0$, $\mu=0$. In conjunction with the above-mentioned energetics, mean-field and Monte Carlo descriptions have been developed in order to study the surface segregation and the kinetics of segregation or dissolution.

B. Mean-field method

The grand-canonical free energy (G) is obtained by averaging both the Hamiltonian (2) and the entropy over all configurations. The simplest (mean-field) approximation is to express the two-site correlation functions $\langle p_n p_m\rangle$ as the product of one-site correlation functions $\langle p_n\rangle\langle p_m\rangle$. Assuming that, in presence of a surface and for a binary alloy A_cB_{1-c}, the concentrations can be different for planes parallel to this surface, one can define i-plane concentrations: $\forall n\in i$ plane, $c_n=\langle p_n\rangle=c_i$. The mean value of G can then

be written $\langle G\rangle=\langle\tilde{H}^{\mathrm{TBIM}}\rangle-T\langle S\rangle$, where $\langle S\rangle$ is the mean value of the entropy calculated in the Bragg-Williams approximation. Its minimization ($d\langle G\rangle/dc_i=0,\forall i$) leads to the following system of coupled nonlinear equations:

$$\frac{c_i}{1-c_i}=\frac{c}{1-c}\exp\left\{-\frac{\Delta H_i}{kT}\right\}. \tag{3}$$

Here c is the bulk concentration, ΔH_i is the segregation energy for the i plane, which is the energy needed to exchange an atom B in the i plane by an atom A from the bulk,

$$\Delta H_0=\Delta\tau+V(Z+2Z')-V_0(Z+Z')+2Z(V_0c_0-Vc)+2Z'(V_0c_1-2Vc),$$

$$\Delta H_1=(V-V_0)Z'+2ZV(c_1-c)+2Z'(V_0c_0+Vc_2-2Vc),$$

$$\Delta H_i=2ZV(c_i-c)+2Z'V(c_{i+1}+c_{i-1}-2c). \tag{4}$$

Equations (3) and (4) are written in concentration of the minority element, i.e., the A deposit. Thus we see that the tendency of the substrate to segregate ($c_0<c$) corresponds to a positive $\Delta\tau$. In Sec. IV A we analyze the equilibrium properties inside the deposit, where the minority elements are the substrate B atoms. We will work in that section in concentration of B and, consequently, the same equations (3) and (4) are used but with $\Delta\tau$ replaced by $-\Delta\tau$. The complete resolution of Eq. (3) using standard numerical methods gives access to the whole possible concentration profiles, including stable, metastable, and unstable solutions. Some simple procedures discussed in a previous work[3] allow us to reach the metastable and stable branches only, which are the pertinent ones in our study.

The kinetics of dissolution is described within the kinetic tight-binding Ising model (KTBIM). This kinetic extension of the TBIM also assumes homogeneous concentrations per plane parallel to the surface and ensures that the steady-state concentration profile corresponds to the equilibrium profile given by Eq. (3). The time dependence of the mean concentration $c_i(t)$ is calculated as a detailed balance between incoming and outcoming fluxes,[22]

$$\frac{\partial c_i}{\partial t}=\frac{1}{t_0}\left[(1-c_i)\left\{\gamma_{i-1}c_{i-1}+\frac{c_{i+1}}{\gamma_i}\right\}-c_i\left\{\frac{(1-c_{i-1})}{\gamma_{i-1}}+\gamma_i(1-c_{i+1})\right\}\right]. \tag{5}$$

γ_i is proportional to the transition probability for an exchange between an A atom in plane i and a B atom in plane $i+1$ and it is related to the instantaneous segregation energies,

$$\gamma_i(t)=\exp\left(\frac{\Delta H_i(t)-\Delta H_{i+1}(t)}{2kT}\right). \tag{6}$$

To each concentration profile satisfying the equilibrium segregation equations (3) corresponds a constant chemical potential referring to the bulk concentration c and equal to

$$\mu=-(Z+2Z')V(1-2c)+kT\ln\frac{c}{1-c}. \tag{7}$$

During the kinetics, a chemical potential gradient appears close to the surface. One may then define instantaneous chemical potentials per i plane,

$$\mu_0(t)=\Delta\tau-(Z+Z')V_0+2V_0[Zc_0(t)+Z'c_1(t)]+kT\ln\frac{c_0(t)}{1-c_0(t)},$$

$$\mu_1(t)=-(Z+Z')V-Z'V_0+2Z'V_0c_0(t)+2V[Zc_1(t)+Z'c_2(t)]+kT\ln\frac{c_1(t)}{1-c_1(t)},$$

$$\mu_i(t)=-(Z+2Z')V+2V\{Zc_i(t)+Z'[c_{i+1}(t)+c_{i-1}(t)]\}+kT\ln\frac{c_i(t)}{1-c_i(t)}. \tag{8}$$

This will allow us to write the following sufficient condition to describe a local equilibrium driven by Eq. (3), between n layers during a period Δt:

$$\forall t\in\Delta t,\quad \mu_0(t)\approx\mu_1(t)\approx\cdots\approx\mu_n(t). \tag{9}$$

C. Monte Carlo method

The Monte Carlo method can also be used in conjunction with the energetics provided by the TBIM to study equilibrium surface segregation and the dissolution kinetics beyond the mean-field approximation. Its realization is performed using the standard Metropolis algorithm, in both canonical and grand-canonical ensembles for equilibrium properties. By varying the chemical potential and for different initial configurations, one can follow the hysteresis (stable and metastable branches) that occurs, for instance, in a first-order layering transition. The canonical calculation which consists in controlling the number of B atoms in a closed system allows us to have a continuous description of the transition with respect to the surface concentration and to determine the critical bulk concentration giving the transition. This method was discussed in detail in a previous work.[3]

By allowing exchanges between first-neighboring atoms only, one can simulate an effective diffusion process and describe the dynamical evolution of the system. For the dissolution of a thick deposit the initial condition mimics the experimental starting condition: a given number of full layers of (minority) A atoms are placed over a substrate of (majority) B atoms. We perform simulations in a box of $(l\times l\times m)$ fcc unit cells with periodic boundary conditions in the directions parallel to the surface plane. In the direction perpendicular to the surface, a free (100) surface is considered on one side while on the opposite side the boundary condition differs according to the type of simulations. For equilibrium ones, to estimate the number of A neighbors outside the simulation box of a given A atom located in the bottom plane we use the same procedure as in Ref. 3. We suppose that the ''virtual'' plane in contact with the simulation box will have the same concentration as the bottom region of the simulation box. Thus, from the last planes we calculate a tentative bulk concentration c_{bottom}, and an A atom located in the bottom plane will have a probability (1

$-c_{bottom})^{Z'}$ to have no A first neighbors in the ''virtual'' plane, a probability $Z' c_{bottom}(1-c_{bottom})^{Z'-1}$ to have one neighboring A atom, etc. Finally we periodically update the tentative c_{bottom} concentration during the simulation. For dissolution kinetics simulations each atom arriving to the bottom plane is removed simulating a $c_m=0$ boundary condition. In this case the choice of the m value could become crucial for thick deposit dissolution. If, for example, the penetration length of A atoms is greater than m, this boundary condition will tend to accelerate the kinetics. However, at the bottom of the simulation box the A concentration is very low and the kinetics is well described using the classical Fick's equations, allowing us to solve this problem. The solution consists of increasing the interlayer distances in order to mimic an effective Fickian region deeper than the penetration length of A atoms. This leads to a correction on the exchange probability proportional to the new effective interlayer distance. In the present work, for $l \approx 20$ and $m \approx 20$ the equilibrium results in the grand-canonical ensemble are independent of the size box. The equilibrium simulations in the canonical ensemble require boxes of larger size: $l \approx 60$ and $m \approx 20$. To avoid any drawback due to the finite size of the box in dissolution kinetics, one must use system sizes such that $l \approx 60$ and $m \approx 1000$. For such dimensions the computing times become too large for performing systematic simulations. We then use lower l values ($l=10,24$), which allows us to extrapolate the results for the larger size.

IV. RESULTS

A. Stable and metastable surface segregation

In this section we explore surface equilibrium behavior as a function of the B bulk concentration c and the surface driving force $\Delta\tau$ for systems presenting a bulk phase separation (AgNi-like: $V=-0.053$ eV) and with a reinforced surface interaction term $V_0=1.5$ V.

Before studying finite-temperature cases, let us perform a simple $T=0$ K analysis, which can be carried out exactly and brings already significant qualitative results. This calculation will give the conditions on $\Delta\tau$ for the occurrence of the stable surface layering sequences. It consists in comparing the ground-state energies of simple configurations which only differ by their number of completed B layers lying on top of the A surface. As we work in concentration of B, the energies are calculated using Eq. (2) with $\Delta\tau$ replaced by $-\Delta\tau$. The energies for n segregated layers $E_n(\mu)$ are

$$E_0(\mu)=0, \quad E_1(\mu)=-\Delta\tau-Z'V_0-\mu,$$

$$E_{n\geq 2}(\mu)=-\Delta\tau-Z'V-n\mu. \tag{10}$$

The linear μ dependence guarantees that the $n=0$ state is preferred for all sufficiently negative μ. Moreover, if a nth-layer transition ($n-1$ layers goes to n layers) occurs, it takes place at a μ value for which $E_{n-1}(\mu)=E_n(\mu)$. Thus, as μ increases to $\mu=0$ [phase separation (PS)] the layering sequence can be

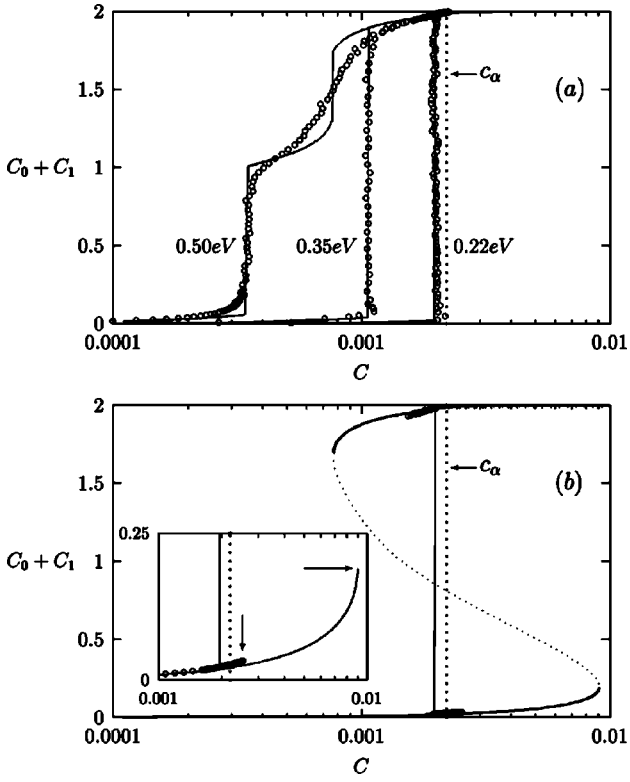

FIG. 3. Equilibrium segregation isotherms in mean field (lines) and Monte Carlo (circles). Sum of the surface c_0 and the subsurface c_1 B concentrations versus the bulk concentration c in logarithmic scale at $T=1200$ K for $V=-0.053$ eV and different values of $\Delta\tau$ for the (100) orientation. (a) Stable states for $\Delta\tau=0.50$, 0.35, and 0.22 eV. (b) Metastable and unstable states for $\Delta\tau=0.22$ eV. The inset shows the lower part of the metastable branches, and the arrows indicate the terminations of these branches where $c=c^0_{l,meta}$.

$$\text{(a)} \quad (0,1,2,\text{PS}) \quad \text{when} \quad \Delta\tau > Z'(V-2V_0),$$

$$\text{(b)} \quad (0,2,\text{PS}) \quad \text{when} \quad Z'(V-2V_0) \geq \Delta\tau > -Z'V,$$

$$\text{(c)} \quad (0,\text{PS}) \quad \text{when} \quad -Z'V \geq \Delta\tau. \tag{11}$$

Note that in terms of multilayer adsorption, $\Delta\tau=-Z'V$ is equivalent to the so-called wetting adatom-substrate interaction u_w (Ref. 15) at $T=0$ K.

The main conclusions found at $T=0$ K remain relevant when performing simulations at $T>0$ K. This is illustrated in Fig. 3, in which we plot for the (100) orientation the sum of the surface and the subsurface concentrations c_0+c_1, issued from both mean-field and Monte Carlo simulations, as a function of the bulk concentration c for three values of $\Delta\tau$, the other parameters being fixed: $V=-0.053$ eV, $V_0=1.5$ V, and $T=1200$ K. In Fig. 3(a), we show the stable branches as the B bulk concentration c increases from 0 to the solubility limit $c_\alpha \approx \exp[(Z+2Z')V/(kT)]=0.0021$. It can be calculated as the bulk concentration for $\mu=0$ in Eq. (7).

(i) The case $\Delta\tau=0.50$ eV corresponds to the layering sequence (a) predicted at $T=0$ K in Eq. (11). This case has been extensively discussed in a previous work.[3] Note that, at $T=1200$ K, the surface and the subsurface layers present first-order transitions in mean-field approximation only. Let us recall that in mean-field approximation, the surface first-

order transition occurs when the temperature is less than $T_l^0 = -ZV_0/2k = 1845$ K, and the subsurface one when the temperature is less than $T_l^1 = -ZV/2k = 1230$ K. In Monte Carlo these critical temperatures (T_l^0 and T_l^1) are lowered by a factor 0.57 for a (100) surface.[23] In addition, the critical bulk concentrations [$c_l^0(T)$ and $c_l^1(T)$] for which these transitions appear can be also derived. At $T=0$ K and from Eq. (10), the first transition takes place when $E_0(\mu)=E_1(\mu)$ which gives $\mu=\mu_l^0=-\Delta\tau-Z'V_0$, and the critical bulk concentration can be derived from Eq. (7), $c_l^0(T) \approx c_\alpha \exp[\mu_l^0/kT]$. Similarly when $E_1(\mu)=E_2(\mu)$, $\mu=\mu_l^1 = Z'(V_0-V)$ and $c_l^1(T)\approx c_\alpha \exp[\mu_l^1/kT]$.

(ii) The calculations for $\Delta\tau=0.35$ eV and 0.22 eV corresponds to case (b) in Eq. (11). In terms of critical bulk concentration the case (b) happens when $c_l^0(T)$ becomes greater than $c_l^1(T)$ in agreement with the $\Delta\tau$ condition established at $T=0$ K. The surface and the subsurface layers go simultaneously from an almost A concentration to an almost B concentration within a first-order transition both in mean-field and in Monte Carlo calculations.

(iii) The latter case corresponds to the absence of layering transitions and is observed when $\Delta\tau \leqslant Z'V = 0.212$ eV.

Let us emphasize that the picture presented here takes into account the stable states only. However, in experiments, particularly at low temperatures where first-order transitions take place, metastable states may dominate the observed behavior. Taking into account the metastable states, we observe the same layering sequences. Nevertheless, the $\Delta\tau$ conditions and the concentration domains of these sequences differ strongly from stable ones and depend on the initial concentration conditions. More precisely, starting from a homogeneous profile, the occurrence of the layering transitions is shifted towards higher bulk concentrations, which extends the range of existence of layering transitions. Therefore, the exploration of the bulk concentration becomes much larger since a solid solution can remain in a metastable state up to the spinodal concentration c_{sp} (above which a bulk phase separation is observed in the simulations). In mean field from the explicit equations for the spinodal line

$$kT = -2(Z+2Z')Vc_{sp}(1-c_{sp}), \tag{12}$$

and for the solubility limit

$$kT = (Z+2Z')V\frac{1-2c_\alpha}{\log\{c_\alpha/(1-2c_\alpha)\}} \tag{13}$$

we obtain at $T=1200$ K, $c_{sp}\approx 50\times c_\alpha$ and we estimate numerically in Monte Carlo $c_{sp}\approx 2.75\times c_\alpha$. In Fig. 3(b) we plot the metastable branches occurring at this temperature for $\Delta\tau=0.22$ eV. Starting from a solid solution and by increasing c we find metastable solutions developed into the miscibility gap. For $c=c_\alpha$ no significant surface enrichment is observed. At the end of the metastable branches one can define critical bulk concentrations analogous to c_l^0 and c_l^1 mentioned above. At $T=1200$ K we find in Fig. 3(b) $c_{l,meta}^0\approx 4.6\times c_l^0$ in mean-field and $c_{l,meta}^0\approx 1.3\times c_l^0$ in Monte Carlo.

Similarly to the stable states study we recover the three possible layering sequences of Eq. (11) but they now depend on the relative values of $c_{l,meta}^0$ and $c_{l,meta}^1$. In mean-field approximation a complete picture describing the metastable transitions can be formulated, if we note that the end of the branches corresponds to precise saddle points occurring in the nonlinear equations [Eq. (3)]. For example, the critical metastable concentration for the surface layer is the maximum value of c for $c_0 \in [0,0.5]$:

$$\left.\frac{\delta c}{\delta c_0}\right|_{c=c_{l,meta}^0} = 0. \tag{14}$$

We will just give here the expression of $c_{l,meta}^0$ since it helps to understand the kinetic phenomena. From Eqs. (3) and (14) we obtain

$$c_{l,meta}^0 \simeq \frac{T_l^0}{T}\left\{1-\sqrt{1-\frac{T}{T_l^0}}\right\}^2 \exp\left\{2\frac{T_l^0}{T}\sqrt{1-\frac{T}{T_l^0}}\right\} c_l^0 . \tag{15}$$

B. Kinetics and local equilibrium in mean-field approximation

This section aims to give a more quantitative description of the kinetic behaviors that we have already qualitatively described in Figs. 1 and 2. The dissolution modes are here described using kinetic mean-field simulations. This simple approach is instructive in that it gives a global picture and brings valuable quantitative information for guiding Monte Carlo simulations. In Sec. IV B 1 the critical temperature T_k delimiting the dissolution domains is determined and the kinetic aspects of the dissolution modes are detailed. In Sec. IV B 2 the T_k line is explained in terms of local equilibrium which allows a quantitative understanding of the phenomenon.

1. Dissolution modes for intermediate-segregation systems

As defined above, the intermediate-segregation systems correspond to systems for which $0<\Delta\tau\sim\Delta\tau_k$, where the difference in both surface energies and atomic radius leads to a segregation of B substrate elements, through the A deposit, up to the surface. This is illustrated in Fig. 4 where we plot the dissolution profiles until the complete dissolution of the deposit into the substrate for 10 ML A/B (100) with $V=-0.053$ eV and $\Delta\tau=0.35$ eV (which corresponds to the Ag-Ni system in the Ni-dilute limit), for two different temperatures below and above T_k. The main difference between the two regimes concerns the behavior of $c_0(t)$ and $c_1(t)$, which either remains close to unity (*layer-by-layer* mode) or vanishes at the beginning of the dissolution process (*surfactant* effect). Therefore, at $T=1200$ K in Fig. 4(a), the A surface concentration $c_0(t)$ oscillates around 0.9, giving a dissolution which proceeds without any significant B enrichment at the surface, while at $T=1250$ K in Fig. 4(b), $c_0(t)$ and $c_1(t)$ decrease rapidly, resulting into two pure capping B monolayers. Note, however, that during this short stage the loss of A matter into the bulk is negligible since the decrease of $c_0(t)$ and $c_1(t)$ is almost perfectly compensated by an increase of $c_{10}(t)$ and $c_{11}(t)$. Then at both temperatures, the concentrations per plane go one by one from pure A to pure B following the sequences described in Fig. 1. Therefore, Fig. 4(a) corresponds to the layer-by-layer mode and Fig. 4(b) to the surfactant-layer-by-layer one.

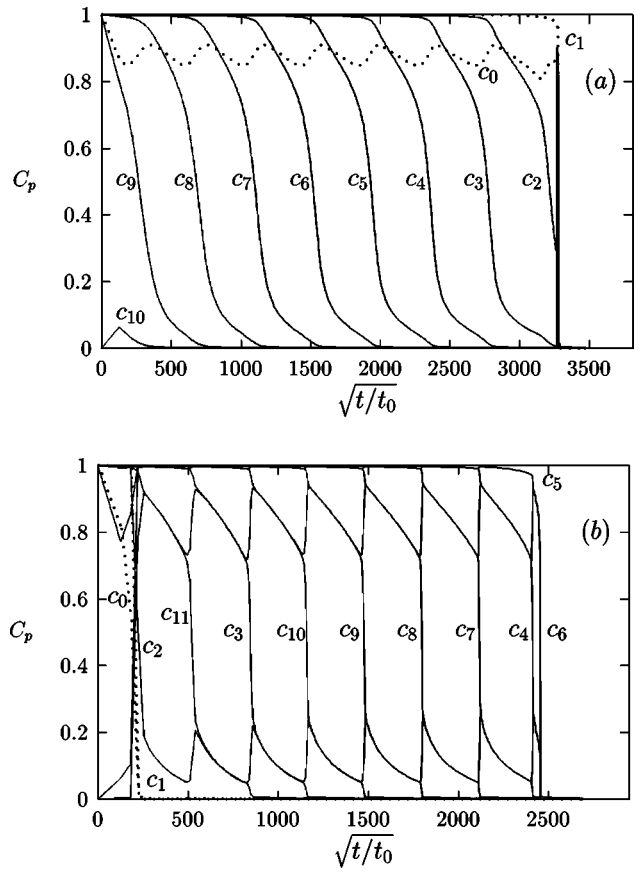

FIG. 4. A layer concentrations c_p versus $\sqrt{t/t_0}$ during the mean-field dissolution of 10 A ML deposited on a B substrate for $V=-0.053$ eV, $\Delta\tau=0.35$ eV, and (a) $T=1200$ K (below T_k) and (b) $T=1250$ K (above T_k). $p=0$: surface layer; $p=1$: subsurface layer, ...

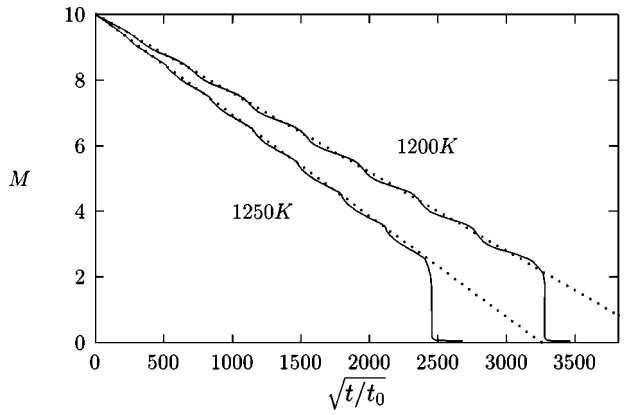

FIG. 5. Sum of the 15 A layer concentrations close to the surface $M(t)$ versus $\sqrt{t/t_0}$ from the dissolution kinetics in Fig. 4 (solid lines). Comparison of the law from Eq. (1) (dotted lines).

In addition, it is clear from Fig. 4 that the distance between any two successive layer transitions is constant in a $\sqrt{t}$ scale. This phenomenon was previously found for the study of 10 ML Ag/Cu,[4] in which case it has been shown that, except for the two surface layers, the loss of deposit matter is driven by the solubility limit and follows a $\sqrt{t}$ law. This behavior was explained by the fact that the instantaneous deposit/substrate interface formed during the dissolution is very close to the equilibrium profile found in an interface of limiting concentrations $1-c_\alpha$ and c_α, where c_α is the solubility limit. Here again, we observe the same feature even if the evolution of the concentration profile can be much more complicated, due to the presence of two A/B interfaces in the surfactant-layer-by-layer mode. This phenomenon is shown in Fig. 5 where we plot the quantity of A matter $M(t)$ in the first 15 layers as a function of the square root of time. The resulting curve oscillates around the one derived for a thick deposit [Eq. (1)] with $M(0)=10$. The validity of such an equation comes from the observation that far from the surface region, A atoms follow a Brownian motion. The flux in A matter from the surface region to the bulk is driven by a particular average concentration [$c_{15}(t)$ in the present case]. When one layer near the surface goes from pure A to pure B, $c_{15}(t)$ oscillates around a constant value which is close to the solubility limit since the instantaneous A/B interface is close to the equilibrium one. Note that the law given by Eq. (1) is due to the strong tendency to phase separation and is independent on surface parameters. This is no longer the case when only two A layers remain close to the surface (see Sec. I).

2. Local equilibrium at T_k

The mean-field simulations have put in evidence the existence of a critical temperature (1200 K$<T_k<$1250 K for $V=-0.053$ eV and $\Delta\tau=0.35$ eV) that delimits two distinct dissolution modes. To explain this transition, we will show in the following that two factors play an important role at the critical temperature: (i) the phenomenon is driven by a local equilibrium between the surface and the deposit/substrate interface, and (ii) the movement of the interface induces a critical B concentration into the deposit leading to a B surface layering transition. Let us now analyze these two points in more detail.

(i) The beginning of the dissolutions shown in Figs. 4 are reported in Fig. 6. At $T=1200$ K$<T_k$, $c_9(t)$ decreases monotonously whereas $c_0(t)$ reaches a minimum [see Fig. 6(a)] while at $T=1250$ K$>T_k$ it is $c_9(t)$ that reaches a minimum whereas $c_0(t)$ decreases monotonously [see Fig. 6(c)]. Thus a signature of the transition may be obtained from the particular evolution of $c_n(t)$ for the two layers which delimit the deposit, namely, $n=0$ (surface) and $n=9$ (interface). In this sense it is only after a specific time corresponding to the occurrence of either one or the other of these minima that we can conclude on the occurrence of the dissolution mode. To understand this behavior at T_k we also plot in Figs. 6(b) and 6(d) the evolution of the chemical potentials per plane, calculated using Eq. (8) from the profiles of Figs. 6(a) and 6(c).

From Fig. 6(b) ($T<T_k$) and when $c_0(t)$ presents a minimum, we observe that the chemical potentials per plane are equal which means, according to Eq. (9), that the kinetics obeys the local equilibrium equations [Eq. (3)]. More precisely, except for the very beginning of the kinetics, the 12 first surface layer concentrations are in local equilibrium during the whole interface layer dissolution, i.e., during the decrease of $c_9(t)$.

From Fig. 6(d) ($T>T_k$), the same conclusions are valid during the first dissolution stage; namely, the chemical potential remains almost homogeneous before the minimum of

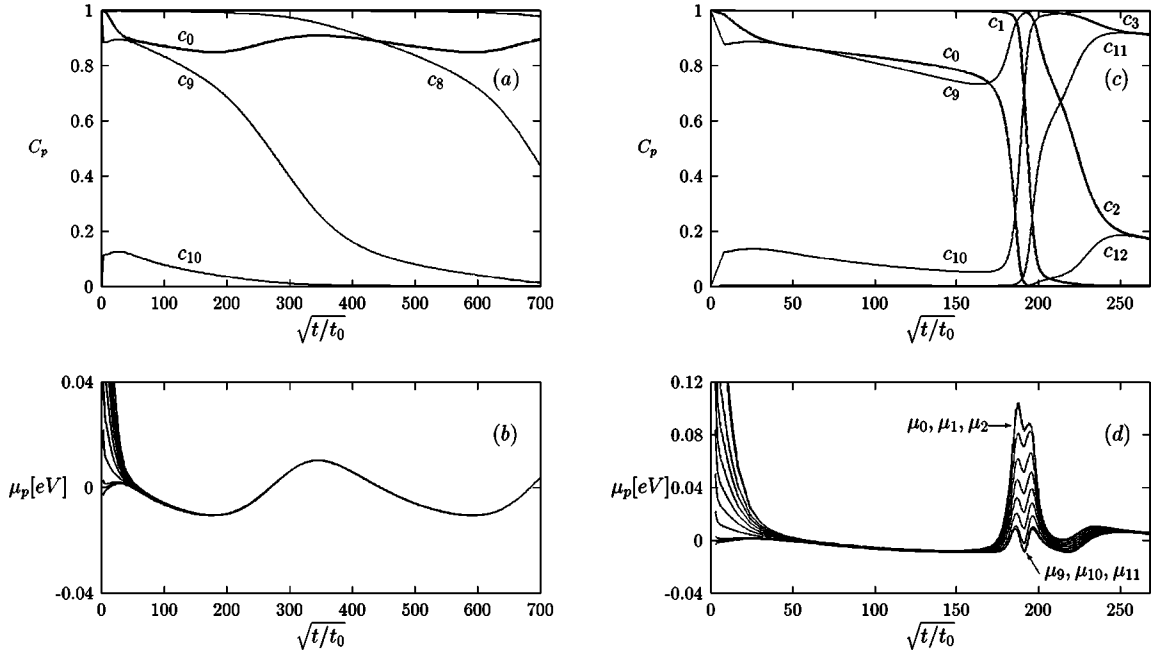

FIG. 6. *A* concentrations c_p and chemical potentials μ_p per plane versus $\sqrt{t/t_0}$ at the very beginning of the dissolutions shown in Fig. 4. (a) and (b) at $T=1200$ K, (c) and (d) at $T=1250$ K.

$c_9(t)$ is reached. Then, once this minimum has been obtained, and during the *B* enrichment of the first two planes (decrease of c_0 and then c_1 down to 0), we notice a large chemical potential gradient into the deposit which separates two regions remaining in local equilibrium, i.e., the surface (c_0,c_1,c_2), and the interface (c_9,c_{10},c_{11}). Finally, once the third surface layer becomes rich in *B* elements, the chemical potentials are equalized which means that the buried *A* film returns into local equilibrium. We can then conclude that, even if the *B* capping (surfactant effect) appears in an off-equilibrium way, the process that initiates this stage and the different layer-by-layer modes are clearly due to a local equilibrium between the deposit layers, including both the surface and the interface regions.Therefore a way to predict the dissolution mode would come from the numerical resolution of the complex system in Eq. (3). By making an exhaustive list of the possible equilibrium profiles, one should then observe, as a function of temperature, the occurrence or the disappearance of a particular solution corresponding to the surfactantlike profile. Practically, in order to reduce the number of equations, it can be performed by fixing the quantity of *A* matter in an adequate finite medium with a judicious choice of the boundary conditions.[24]

(ii) An additional observation will allow us to simplify the problem and to describe this transition in a more general way, in terms of surface segregation with a particular bulk concentration due to the interface movement. In the kinetic range driven by local equilibrium equations and for temperatures above and below T_k, the homogeneity of the chemical potential means the absence of a concentration gradient within the deposit: $c_3(t)\simeq c_4(t)\simeq\cdots\simeq c_8(t)$. This allows us to separate the deposit in two distinct regions where the local equilibrium applies: one region controlled by the surface isotherms (discussed in detail in Sec. IV A) and the other controlled by the interface only. Thus, if the whole kinetic profile looks like the above-mentioned profiles of these two separated regions at $T=T_k$, then the transition may be understood. This local equilibrium concept leads us to consider the instantaneous kinetic profile as formed by the profiles of two systems almost in equilibrium connected through only one concentration (c_3). We can then plot the two equilibrium isotherms, at the surface: $c_0(c_3)$ and at the interface: $c_9(c_3)$, in order to see if the kinetics follow them or not.

In Fig. 7(a), we show the equilibrium *B* surface concentration c_0 versus the concentration of the fourth plane c_3 from the surface segregation isotherm compared to the relation between these two concentrations issued from the kinetics at a temperature below T_k. Figure 7(c) presents the same comparison for a temperature above T_k. At both temperatures, we notice that the surface isotherms present the van der Waals loop related to a first-order transition at the surface. At $T<T_k$ in Fig. 7(a), $c_3(t)$ is lower than $c^0_{l,meta}$ and therefore no strong *B* surface enrichment takes place. Conversely at $T>T_k$ in Fig. 7(c), $c_3(t)$ is larger than $c^0_{l,meta}$ giving the surfactantlike effect. Nevertheless, even though the relative positions of $c_3(t)$ and $c^0_{l,meta}$ indeed give the signature of the phenomenon and allow us to relate T_k to $c^0_{l,meta}$, we have not yet explained how the concentration in the *B* element in the deposit $c_3(t)$ can be greater than $c^0_{l,meta}$ and also greater than c_α. It requires us to look at what happens at the other limit of the deposit, i.e., to consider the local equilibrium induced by the interface.

To calculate the interface isotherms, one builds a sharp interface by starting from an initial condition consisting of two pure separated blocks. We impose two boundary conditions $c_i=c_{i+1}$ on each side far from the interface region to ensure that no concentration gradient occurs. By controlling the concentration of the first plane rich in *A* at the interface, representing here the tenth plane c_9 in the dissolution kinetics, the system is then equilibrated and constant concentrations c_f and $(1-c_f)$ are found at each side of the interface.

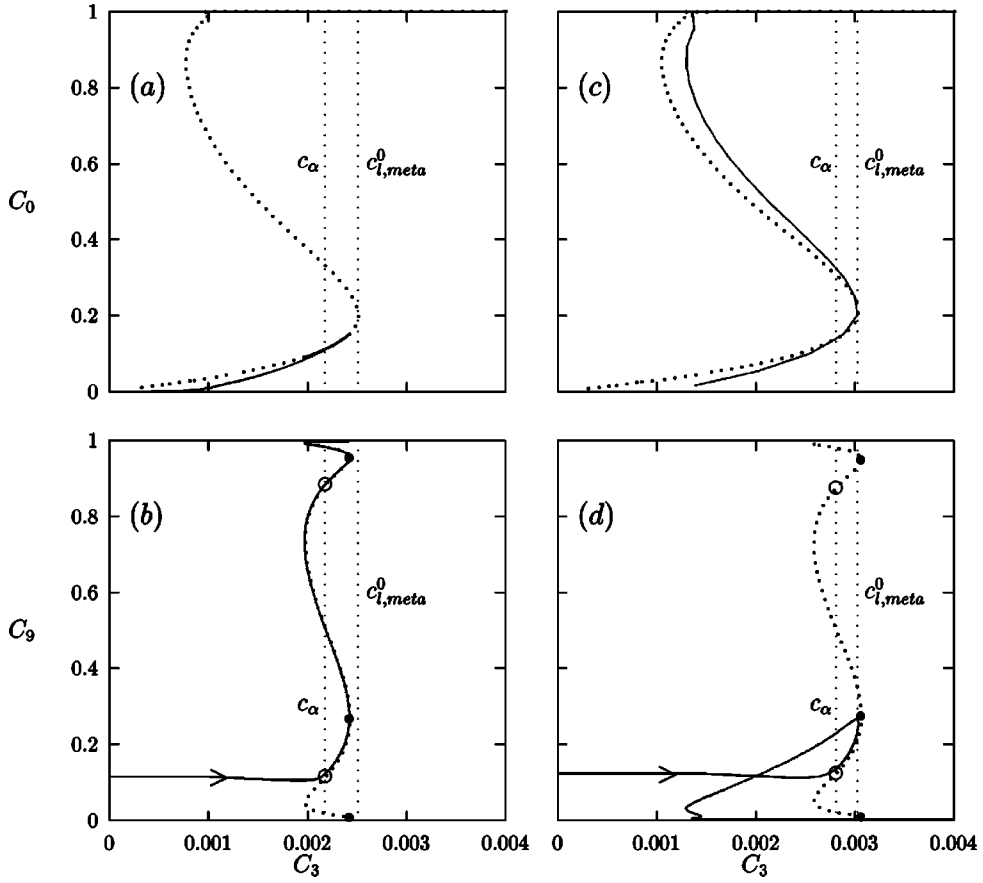

FIG. 7. Mean-field equilibrium surface segregation and interphase isotherms (dotted lines) compared to the dissolution kinetics (solid lines) shown in Fig. 6. (a) c_0 vs c_3 from the surface isotherms at $T=1200$ K, (b) c_9 vs c_3 from the interface isotherms at $T=1200$ K, (c) c_0 vs c_3 from the surface isotherms at $T=1250$ K, and (d) c_9 vs c_3 from the interface isotherms at $T=1250$ K. The vertical dotted lines show the position of $c^0_{l,meta}$ and c_α. All the concentrations are in element *B*.

This constant concentration c_f which depends on c_9 leads us to an equilibrium relation $c_9(c_f)$. This relation will be compared to the kinetic relation $c_9(c_3)$. In this sense we report in Figs. 7(b) and 7(d) the resulting c_9 versus c_f curves at both temperatures, below and above T_k. The usual way to calculate the interface profile is to keep the boundary conditions constant and equal to c_α and $1-c_\alpha$. Here by fixing c_9, we impose the position of the interface on the discrete lattice. Its stabilization may give stable and metastable profiles for which the concentration far from the interface c_f may differ from c_α. In Figs. 7(b) and 7(d) we observe that when c_9 goes from pure *A* to pure *B* (here from 0 to 1), c_f oscillates around the solubility limit c_α. This curve points out well-known results concerning the equilibrium discrete shape of a planar interface. Indeed, we recover here the two well-known profiles corresponding to $c_f=c_\alpha$. One of these solutions is reached when the concentrations per plane are symmetrical with respect to 0.5 so that $c_9=1-c_8$ (or $c_9=1-c_{10}$), the other one when $c_9=0.5$. However when the center of the interface is located between these two particular discrete profiles ($0.2<c_9<0.5$), c_f presents a maximum value c_f^{max} greater than the solubility limit c_α.

Let us now examine the kinetics at the light of these equilibrium results. At $T=1200$ K in Fig. 7(b), we notice that the relation $c_9(c_3)$ derived from the kinetics follows the relation $c_9(c_f)$ derived from the equilibrium. During the layer-by-layer mode $c_9(t)$ increases continuously from 0 to 1. This displacement of the interface induces important oscillations of concentration in *B* elements in the deposit $[c_3(t)]$ which, however, are not sufficient to provoke the *B* surface enrichment. In terms of local equilibrium, it can be formulated by the relation $c_f^{max}(c_9)<c^0_{l,meta}$. At $T=1250$ K in Fig. 7(d) we obtain that $c_f^{max}(c_9)$ is greater than $c^0_{l,meta}$. This gives a $c_3(t)$ value greater than $c^0_{l,meta}$ and therefore an irreversible *B* surface enrichment. Then, once $c^0_{l,meta}$ has been reached, the kinetics follows an off-equilibrium path consistently with the previous chemical potential analysis. As a conclusion, the change of the dissolution mode occurs at a critical temperature corresponding to the equilibrium relation

$$c_f^{max}(c_9)=c^0_{l,meta}. \tag{16}$$

In Fig. 8 we show results of systematic mean-field simulations of 10-ML dissolution in order to determine the T_k line as a function of $\Delta\tau$ for $V=-0.053$ eV (which corresponds to the Ag-Ni system). Also reported on this graph is the curve for which the $(\Delta\tau,T)$ couple satisfies numerically the equilibrium condition of Eq. (16) for the same value of *V*.

At low temperature, it is possible to deal with Eq. (16) and to derive an approximate analytical expression of T_k vs $\Delta\tau$. From this expression we can also calculate $\Delta\tau_k$ which delimits the frontier between the intermediate segregation regime and the strong one where only the surfactant-layer-by-layer mode occurs. From Eq. (3), we can estimate

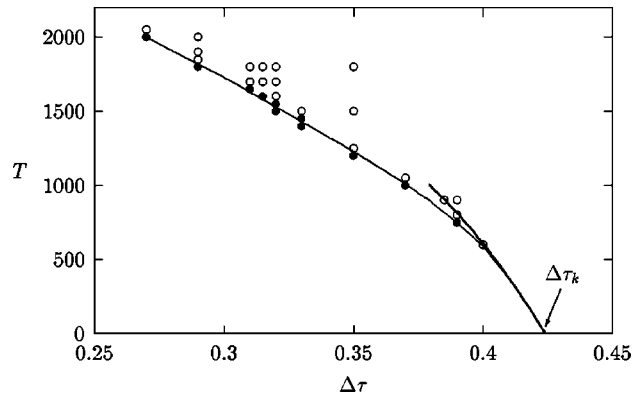

FIG. 8. Mean-field map showing the critical temperature T_k versus $\Delta\tau$ that separates the regions where the two dissolution modes occur. The filled circles (●) correspond to simulations where the layer-by-layer dissolution mode occurred and the open circles (○) to simulation presenting a surfactantlike dissolution mode. The solid line is the numerical $T_k(\Delta\tau)$ line calculated using Eq. (16) and the dashed line is the low-temperature derivation of the $T_k(\Delta\tau)$ line [Eq. (18)].

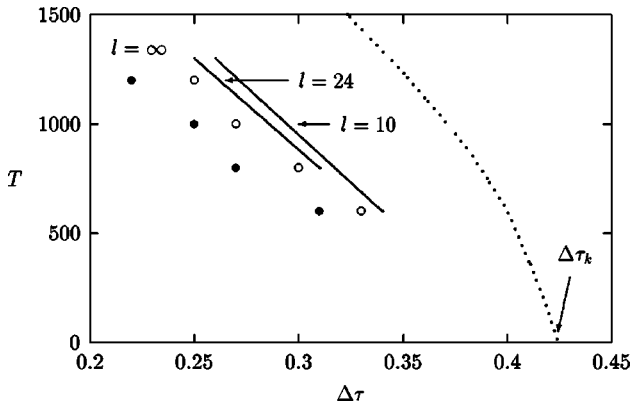

FIG. 9. Monte Carlo map showing the critical temperature T_k versus $\Delta\tau$ that separate the regions where the two dissolution modes occur. The solid lines correspond to the T_k lines obtained from the kinetic Monte Carlo simulations for two different lateral sizes of the simulation box l. The open (○) and filled (●) circles delimit the region where we estimate the occurrence of the T_k line for $l=\infty$ (see text). The dotted line is the numerical $T_k(\Delta\tau)$ line calculated using Eq. (16).

$c_f^{max}(c_9)$ by assuming that at low temperature the interface is very sharp and $c_8+c_{10}\approx 1$. This gives c_f as a function of c_9 only. Differentiating c_f with respect to c_9 we obtain

$$c_f^{max}(c_9)=\frac{T_l^1}{T}\left\{1-\sqrt{1-\frac{T}{T_l^1}}\right\}^2 \exp\left\{2\frac{T_l^1}{T}\sqrt{1-\frac{T}{T_l^1}}\right\} c_\alpha . \tag{17}$$

Then from Eqs. (15), (16), and (17) we get

$$\frac{-\Delta\tau}{2kT}=\ln\left\{\frac{\sqrt{T_l^0}-\sqrt{T_l^0-T}}{\sqrt{T_l^1}-\sqrt{T_l^1-T}}\right\}+\frac{T_l^0}{T}\left\{\frac{Z'}{Z}+\sqrt{1-\frac{T}{T_l^0}}\right\} -\frac{T_l^1}{T}\left\{\sqrt{1-\frac{T}{T_l^1}}\right\}. \tag{18}$$

In Fig. 8 we show that this expression fits very well the numerical T_k line up to 700 K. As mentioned above, we can calculate from Eq. (18) for $T=0$ K the limiting value of the surface segregation term: $\Delta\tau_k=-(Z'+Z)V_0+ZV$. The mean-field approach is exact at $T=0$ K; this latter result should also be relevant in the Monte Carlo simulations.

C. Kinetics and local equilibrium in Monte Carlo simulations

Kinetic Monte Carlo simulations allow us to take into account thermal fluctuations which are neglected in the mean-field approximation. These fluctuations tend to disorder the system and then to reduce the temperature at which the transition occurs. Thus, from the considerations on surface segregation in Sec. IV A one can expect the same kinetic phenomena in a temperature range reduced by a factor 0.57 for the (100) orientation.[23]

1. Dissolution modes for intermediate-segregation systems

The Monte Carlo map for the different modes of dissolution is shown in Fig. 9 for a deposit of 10 ML and for $V=-0.053$ eV. We recover qualitatively the same picture established from the mean-field calculations. However the T_k line is now lowered and depends on the lateral size l of the simulation box. For $l=10$ and $l=24$, the computing times are still reasonable to allow the determination of the dissolution mode in a wide range of temperatures. We find that increasing the lateral size of the box tends to lower the position of the T_k line. The asymptotic value is also shown in Fig. 9, as calculated in the next section.

2. Local equilibrium at T_k

The mean-field analysis of T_k in terms of local equilibrium can be extended to interpret the Monte Carlo results. However, an additional problem arises here related to the size box dependence of the kinetic results. To understand the kinetic transition it is necessary to perform surface equilibrium simulations depending also on the lateral size of the box l. We have performed these simulations in the canonical ensemble as described in Sec. III C. Thus, by analogy with the mean-field approach and for a given l we compare concentrations per plane obtained from the equilibrium simulations in the canonical ensemble and from the kinetics. In Fig. 10 we plot c_0 versus c_4, above and below T_k, for a (100) surface with $l=24$, $V=-0.053$ eV, and $\Delta\tau=0.27$ eV. At both temperatures the surface isotherms present metastable branches that penetrate into the miscibility gap. When the concentration in B elements in the deposit $c_4(t)$ reaches the termination of these branches $c_{l,meta}^0$, three-dimensional (3D) B clusters grow rapidly in the first surface planes until they cover the deposit by pure B capping layers. When $c_4(t)<c_{l,meta}^0$ the surface kinetics remains in a metastable state consisting of very small two-dimensional (2D) B islands formed in the surface plane only [$c_0(t)\simeq 0.04$ at $T=1100$ K]. Regarding the l dependence of $c_{l,meta}^0$, one can estimate the ''real'' T_k line. From equilibrium simulations we note that when l increases $c_{l,meta}^0$ decreases. In other words, the critical size of the 2D B germs giving the surfactant effect decreases for larger lateral size. Consequently the necessary value for $c_4(t)$, and therefore the corresponding

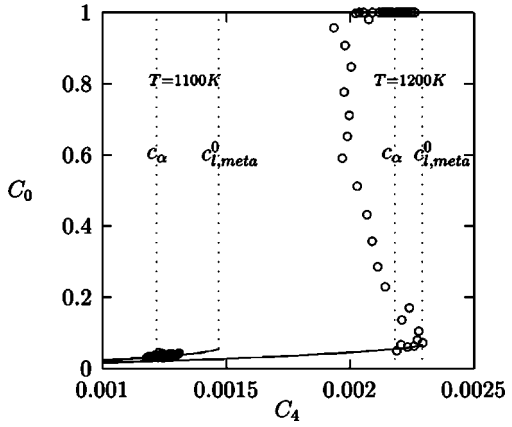

FIG. 10. Monte Carlo equilibrium surface segregation (solid lines) compared to the dissolution kinetics (circles) for two different temperatures $T=1100$ K$<T_k$ and $T=1200$ K$>T_k$. $l=24$, $V=-0.053$ eV, and $\Delta\tau=0.27$ eV. Surface concentration c_0 vs the concentration of the fifth layer c_4.

temperature, to obtain the transition is lowered. This gives $T_k(l=10)>T_k(l=24)>T_k(l=\infty)$ as observed in Fig. 9. The mechanism of the transition being clearly identified, we can now search the $T_k(\Delta\tau)$ line corresponding to $l=\infty$. We use the surface equilibrium results obtained in the grand canonical from Sec. IV A where no size box effect takes place. For a given temperature, the maximum value of $\Delta\tau[T_k(l=\infty)]$ is chosen so that $c^0_{l,meta}=c_\alpha$, which ensures the occurrence of the surfactant-layer-by-layer mode. Concerning the minimum boundary below where we should observe a layer-by-layer mode only, we have taken $\Delta\tau[T_k(l=\infty)]$ so that $c^0_{l,meta}>3c_\alpha$ for 600 K$<T_k(l=\infty)<$1200 K. This estimation is valid for the equilibrium mean-field interface (see Sec. IV B 2) and it is also consistent with kinetic results obtained for $l=10$ and $l=24$. The resulting $T_k(l=\infty)$ region as a function of $\Delta\tau$ is plotted in Fig. 9. It is relatively confined and presents the interesting property to converge towards $\Delta\tau_k$ derived at $T=0$ K from the mean-field analysis.

V. DISCUSSION AND CONCLUSION

In this paper we have studied the dissolution of a thick A metal film into a B metal substrate in the case where the corresponding AB alloy presents a tendency to bulk phase separation and to B surface segregation. The energetic model used in this work is an Ising Hamiltonian whose parameters were obtained from semiempirical tight-binding calculations. This energetic model allowed us to obtain the equilibrium segregation properties of the alloy. The same energetic parameters were used to study the kinetic behavior, which is obtained using an extension of this model, the kinetic tight-binding Ising model. Either in the mean-field or in the Monte Carlo framework, we have found layer-by-layer dissolution modes which, depending on the annealing temperature T, are preceded ($T>T_k$) or not ($T<T_k$) by the rising of capping B monolayers burying an almost intact A film (surfactantlike effect). We have found that T_k decreases as the tendency to surface segregation of the substrate element increases (more positive $\Delta\tau$). We have succeeded in explaining this behavior in terms of local equilibrium at both the surface and the interface of the deposit. We have also found that the quantity of deposit matter decreases linearly with the square root of time, during both dissolution modes, and that in the high-temperature mode, the surface enrichment in substrate element increases linearly with time.

In the model $\Delta\tau$ is defined as the resulting contribution of both the difference in surface energies Δh_0^{eff} and the possible size mismatch between the two constituents ΔH_0^{size}. The calculation of the ΔH_0^{size} term shows that the size effect should induce a segregation of the impurity at surface only if it is the largest. The value of such a term has been previously discussed (see Ref. 25) for phase separation systems when the impurity is the largest element. The authors have put in evidence that the size effect ΔH_0^{size} strongly depends on the surface concentration c_0 and thus can drastically modify the first layering transition in the segregation process. More precisely, they found for the segregation of Ag on Cu(111) that ΔH_0^{size} is strongly reduced when the stress is partially relaxed by the formation of a (9×9) superstructure. We are aware that the present model, which relies on a rigid lattice assumption, does not take into account in a proper way these atomic displacements. Accounting for this effect requires one to develop a kinetic Monte Carlo algorithm allowing atomic displacements, estimated by using a realistic interatomic potential. This is an important task which will be the subject of a future work. Nevertheless, we think that the simple rigid lattice model used in this work can give access to valuable information on the microstructure of the metastable profiles. For example, in what concerns the influence of the deposit thickness for ''Ni/Ag-like'' systems, we expect that a critical deposit size should give rise to either a clustering as predicted in a previous work[8] (thin deposit case) or to planar interfaces as mentioned here (thick deposit case).

Moreover, in what concerns the general result shown in Fig. 2, it can be directly compared to experimental works performed on systems of the Ni/Ag type, but which present a significantly lower size-mismatch. This is the case, for instance, of the Fe/Cu system which, according to its energetic parameters, should be classified in the intermediate segregation regime. Indeed, using low-energy ion scattering, Detzel and Memmel[10] have recently analyzed the change of surface composition as a function of temperature and of the initial Fe film thickness. For a Fe coverage greater than 6 ML, the authors do not notice any modifications in the surface composition for annealing temperatures below 420 K. However, at slightly higher values, they detect a drastic increase of the Cu surface concentration corresponding to at least two monolayers. These experimental results can then be directly connected to the transition shown in the present paper.

ACKNOWLEDGMENTS

It is a pleasure to thank S. Delage and F. Soisson (SRMP, CEA Saclay) for very valuable discussions on the different layer-by-layer dissolution modes and on the surfactant effect.

[1] U. Bardi, Rep. Prog. Phys. **57**, 939 (1994).
[2] J. Eugène, B. Aufray, and F. Cabané, Surf. Sci. **241**, 1 (1991).
[3] A. Saúl, B. Legrand, and G. Tréglia, Phys. Rev. B **50**, 1912 (1994).
[4] A. Saúl, Mater. Sci. Forum **155/156**, 233 (1994); A. Saúl, B. Legrand, and G. Tréglia, Surf. Sci. **331-333**, 805 (1995).
[5] B. Aufray, H. Giordano, B. Legrand, and G. Tréglia, Surf. Sci. **307-309**, 531 (1994).
[6] C. Nagl, E. Platzgummer, M. Schmid, P. Varga, S. Speller, and W. Heiland, Phys. Rev. Lett. **75**, 2976 (1995); Surf. Sci. **352-354**, 540 (1996).
[7] K.S. Lee, S.H. Kim, H.G. Min, Jikeun Seo, and Jae-Sung Kim, Surf. Sci. **377-379**, 918 (1997).
[8] J.M. Roussel, A. Saúl, G. Tréglia, and B. Legrand, Phys. Rev. B **55**, 10 931 (1997).
[9] P.J. Schmitz, W.Y. Leung, G.W. Graham, and P.A. Thiel, Phys. Rev. B **40**, 11 477 (1989).
[10] Th. Detzel and N. Memmel, Phys. Rev. B **49**, 5599 (1994).
[11] Li Hong and B.P. Tonner, Surf. Sci. **237**, 141 (1990).
[12] A.K. Schmid, D. Atlan, H. Itoh, B. Heinrich, T. Ichinokawa, and J. Kirschner, Phys. Rev. B **48**, 2855 (1993).
[13] A. Senhaji, G. Tréglia, B. Legrand, N.T. Barrett, C. Guillot, and B. Villette, Surf. Sci. **274**, 297 (1992).
[14] A. Senhaji, G. Tréglia, J. Eugène, A. Khoutami, and B. Legrand, Surf. Sci. **287/288**, 371 (1993).
[15] R. Pandit, M. Shick, and M. Wortis, Phys. Rev. B **26**, 5112 (1982).
[16] M. Laguës and J.L. Dommange, Surf. Sci. **47**, 77 (1975).
[17] J.M. Roussel, A. Saúl, G. Tréglia, and B. Legrand (unpublished).
[18] A. Bieber, F. Gautier, G. Tréglia, and F. Ducastelle, Solid State Commun. **39**, 149 (1981).
[19] G. Tréglia, B. Legrand, and F. Ducastelle, Europhys. Lett. **7**, 575 (1988).
[20] D. Tománek, A.A. Aligia, and C.A. Balseiro, Phys. Rev. B **32**, 5051 (1985).
[21] G. Tréglia and B. Legrand, Phys. Rev. B **35**, 4338 (1987).
[22] G. Martin, Phys. Rev. B **41**, 2279 (1990).
[23] See, for example, M.E. Fisher, Rep. Prog. Phys. **30**, 615 (1967).
[24] S. Delage, B. Legrand, F. Soisson, and A. Saúl, Phys. Rev. B **58**, 15 810 (1998).
[25] G. Tréglia, B. Legrand, J. Eugène, B. Aufray, and F. Cabané, Phys. Rev. B **44**, 5842 (1991).